Supplementary information for: Cheater suppression and spite through quorum sensing

Alexander S. Moffett[a], Peter J. Thomas[b], Michael Hinczewski[c], and Andrew W. Eckford[a,1]

[a]Department of Electrical Engineering and Computer Science, York University, Toronto, Ontario M3J 1P3, Canada
[b]Department of Mathematics, Applied Mathematics, and Statistics, Case Western Reserve University, Cleveland, Ohio 44106, USA
[c]Department of Physics, Case Western Reserve University, Cleveland, Ohio 44106, USA

June 16, 2021

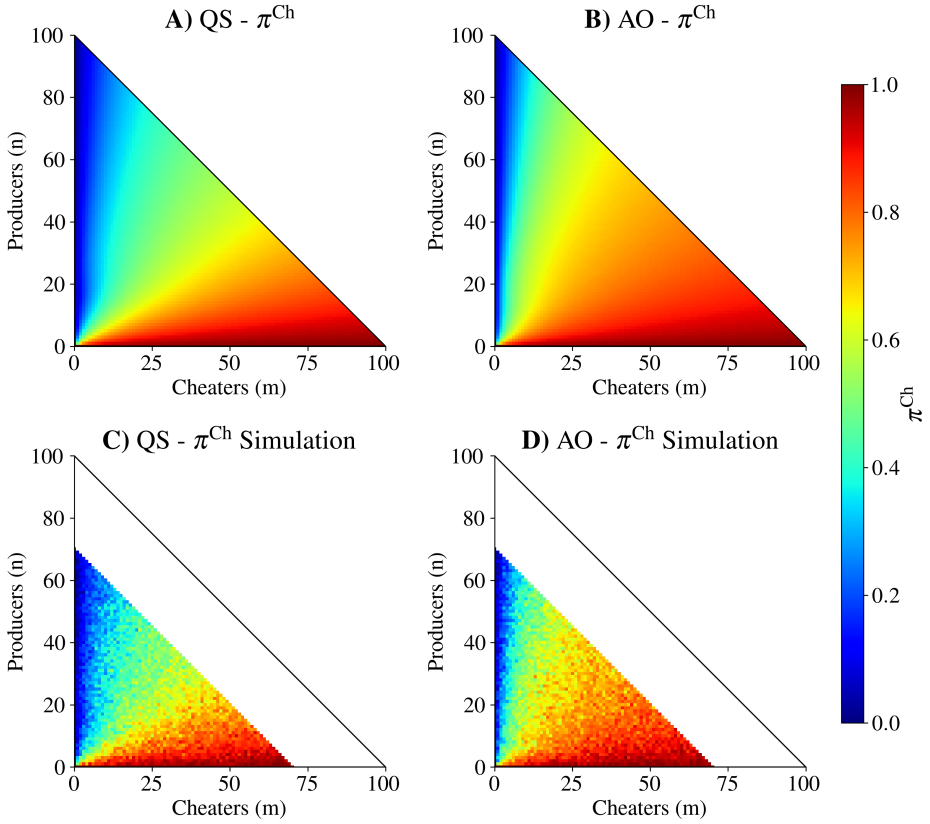

Figure S1: The cheater fixation probabilities from Fig 2 agree with simulation results. The first row shows the cheater fixation probabilities for A) quorum sensing (QS) and B) always on (AO) strategies, directly reproduced from Fig. 2. The second row shows cheater fixation probabilities calculated as a mean from 100 independent simulations for C) QS and D) AO strategies. Points above $n + m = 70$ (above the zero-net growth contour) were not calculated. See Table S2 for parameter values.

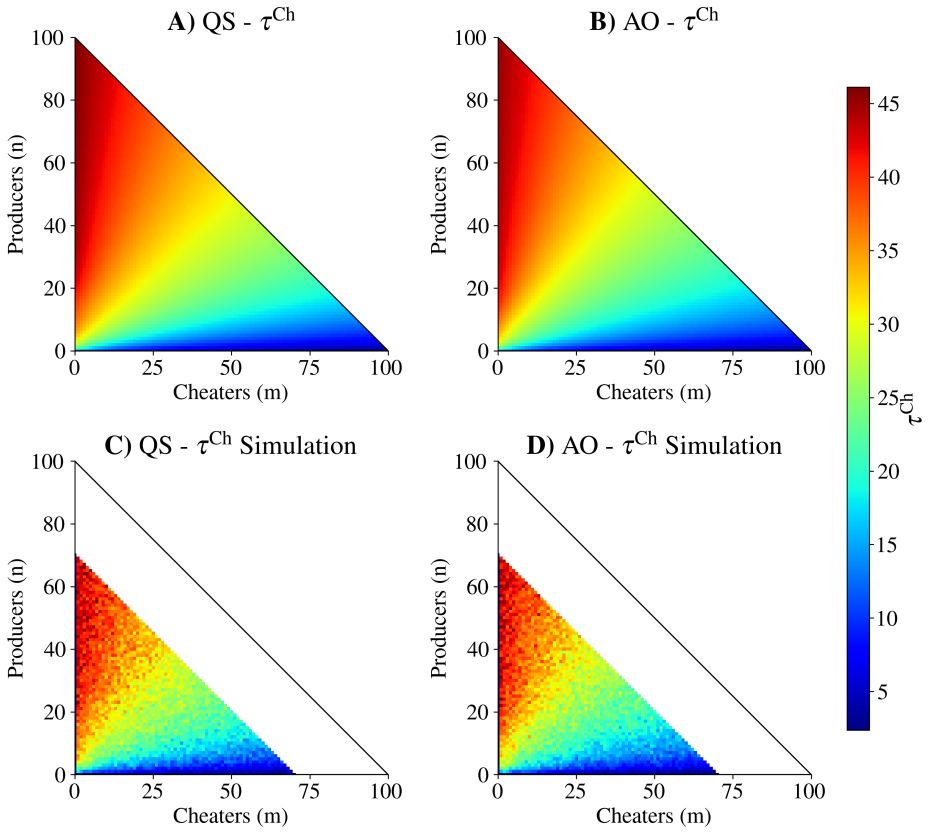

Figure S2: The cheater mean first passage time to fixation from Fig 2 agree with simulation results. The first row shows the cheater fixation mean first passage times for A) quorum sensing (QS) and B) always on (AO) strategies, directly reproduced from Fig. 2. The second row shows cheater fixation mean first passage times calculated as a mean from 100 independent simulations for C) QS and D) AO strategies. Points above $n + m = 70$ (above the zero-net growth contour) were not calculated. See Table S2 for parameter values.

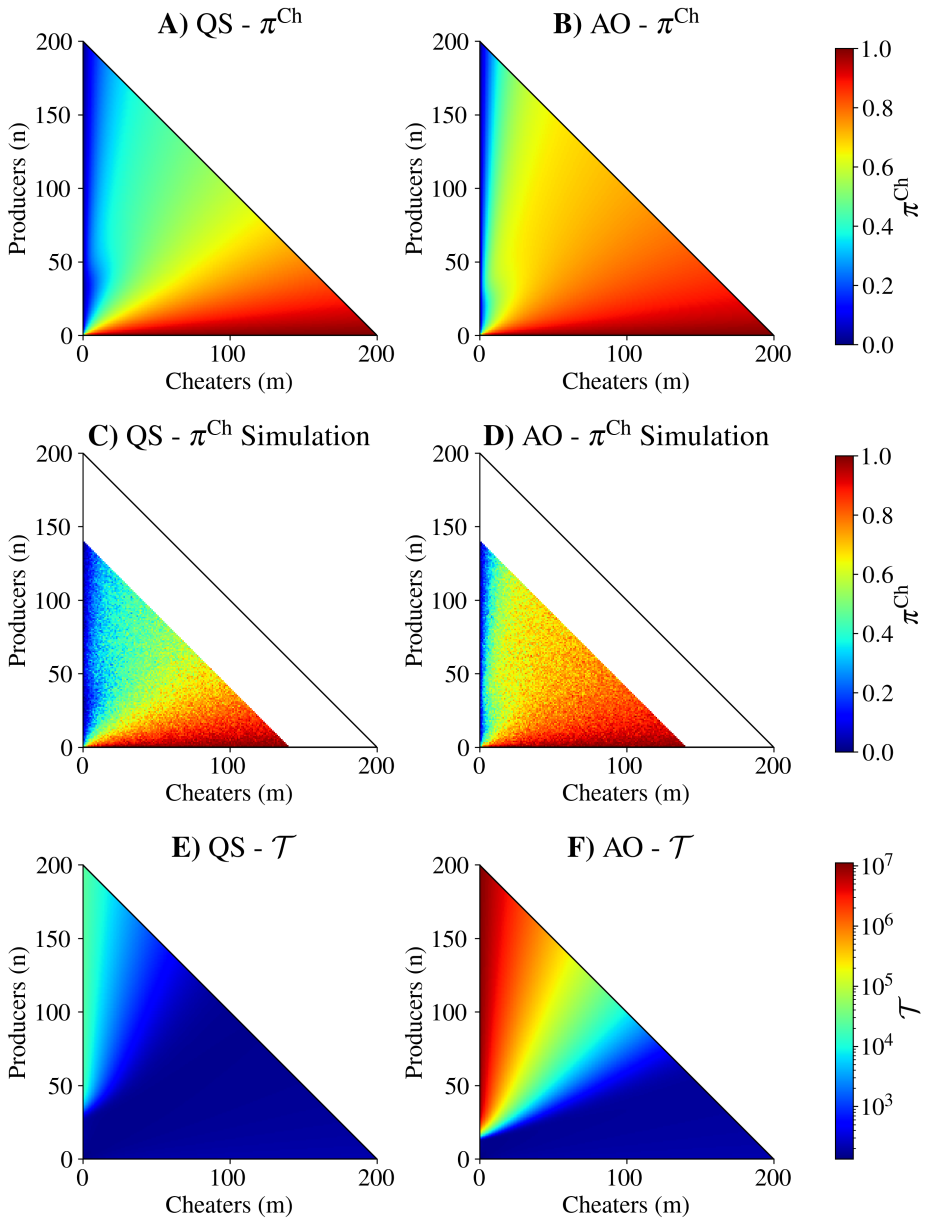

Figure S3: The qualitative results from Fig. 2 are preserved with increased carrying capacity, with no constitutive growth (λ_0). The first row depicts cheater fixation probability from an initial population structure of n producers and m cheaters for A) quorum sensing (QS) and B) always on (AO) strategies. The second row depicts cheater fixation probabilities calculated as a mean of 100 independent simulations for C) QS and D) AO strategies. Points above $n + m = 140$ (above the zero-net growth contour) were not calculated. The third row depicts mean extinction time from initial population structure for E) QS and F) AO strategies, calculated according to Eq. 19. As with the results in Fig. 2, QS decreases cheater fixation probability but also decreases mean extinction time as compared with AO. See Table S2 for parameter values.

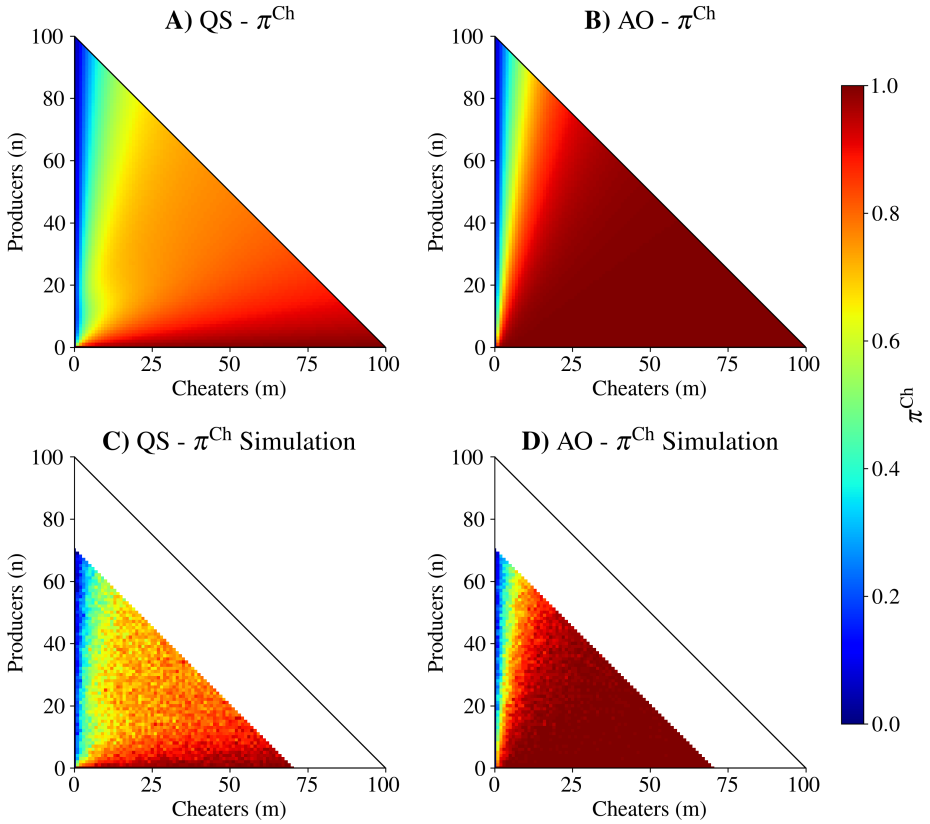

Figure S4: The cheater fixation probabilities from Fig 3 agree with simulation results. The first row shows the cheater fixation probabilities for A) quorum sensing (QS) and B) always on (AO) strategies, directly reproduced from Fig. 3. The second row shows cheater fixation probabilities calculated as a mean from 100 independent simulations for C) QS and D) AO strategies. Points above $n + m = 70$ (above the zero-net growth contour) were not calculated. See Table S2 for parameter values.

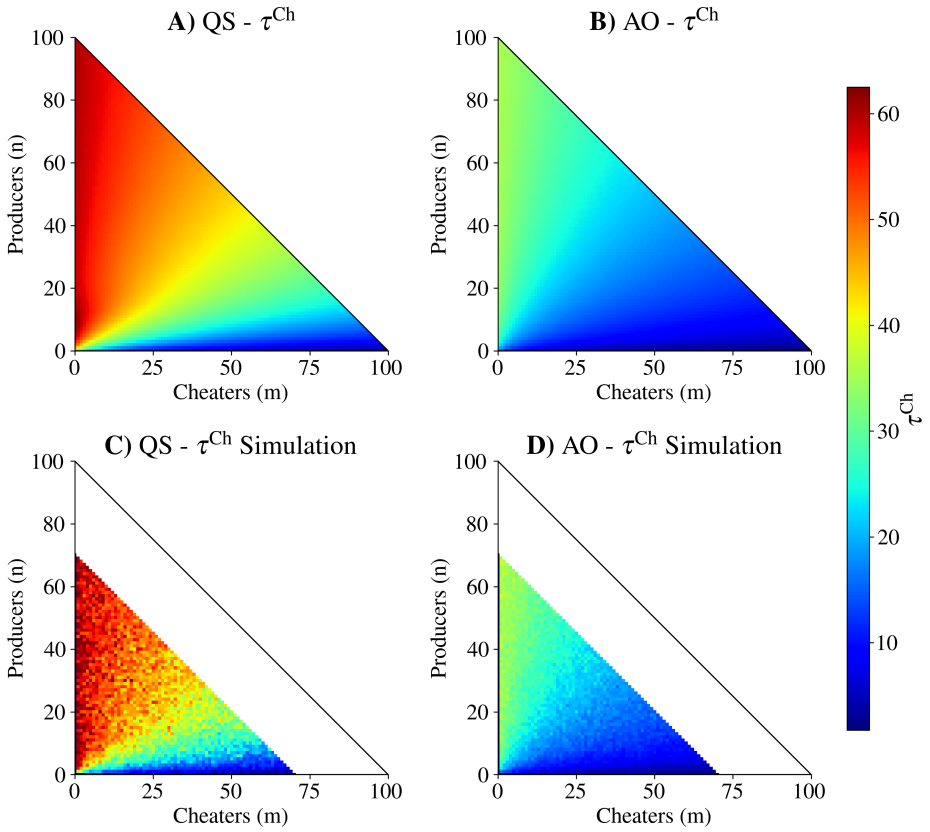

Figure S5: The cheater mean first passage time to fixation from Fig 3 agree with simulation results. The first row shows the cheater fixation mean first passage times for A) quorum sensing (QS) and B) always on (AO) strategies, directly reproduced from Fig. 3. The second row shows cheater fixation mean first passage times calculated as a mean from 100 independent simulations for C) QS and D) AO strategies. Points above $n + m = 70$ (above the zero-net growth contour) were not calculated. See Table S2 for parameter values.

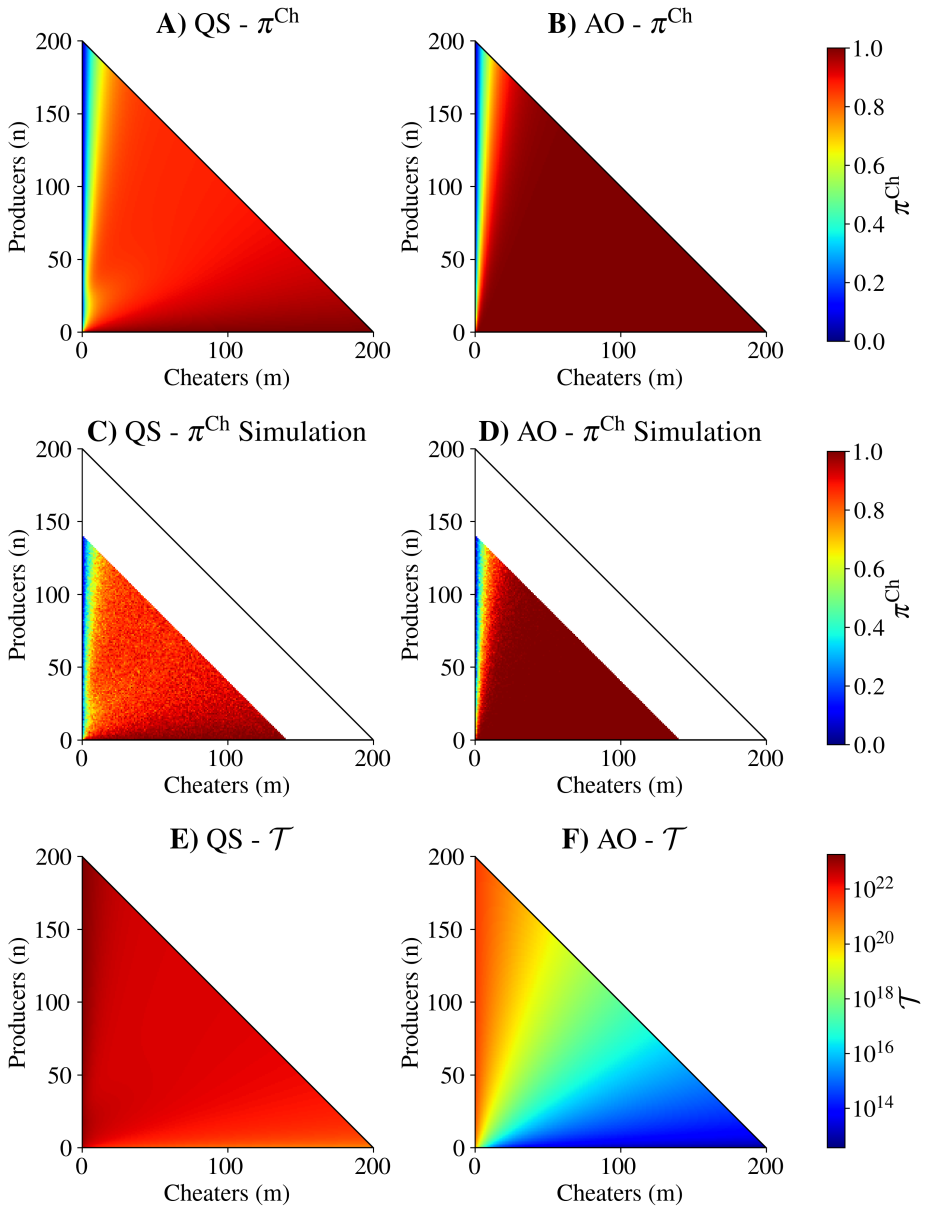

Figure S6: The qualitative results from Fig. 3 are preserved with increased carrying capacity, with constitutive growth ($\lambda_0 = 0.2$). The first row depicts cheater fixation probability from an initial population structure of n producers and m cheaters for A) quorum sensing (QS) and B) always on (AO) strategies. The second row depicts cheater fixation probabilities calculated as a mean of 100 independent simulations for C) QS and D) AO strategies. Points above $n + m = 140$ (above the zero-net growth contour) were not calculated. The third row depicts mean extinction time from initial population structure for E) QS and F) AO strategies, calculated according to Eq. 19. As with the results in Fig. 3, QS decreases cheater fixation probability while also increasing mean extinction time as compared with AO. See Table S2 for parameter values.

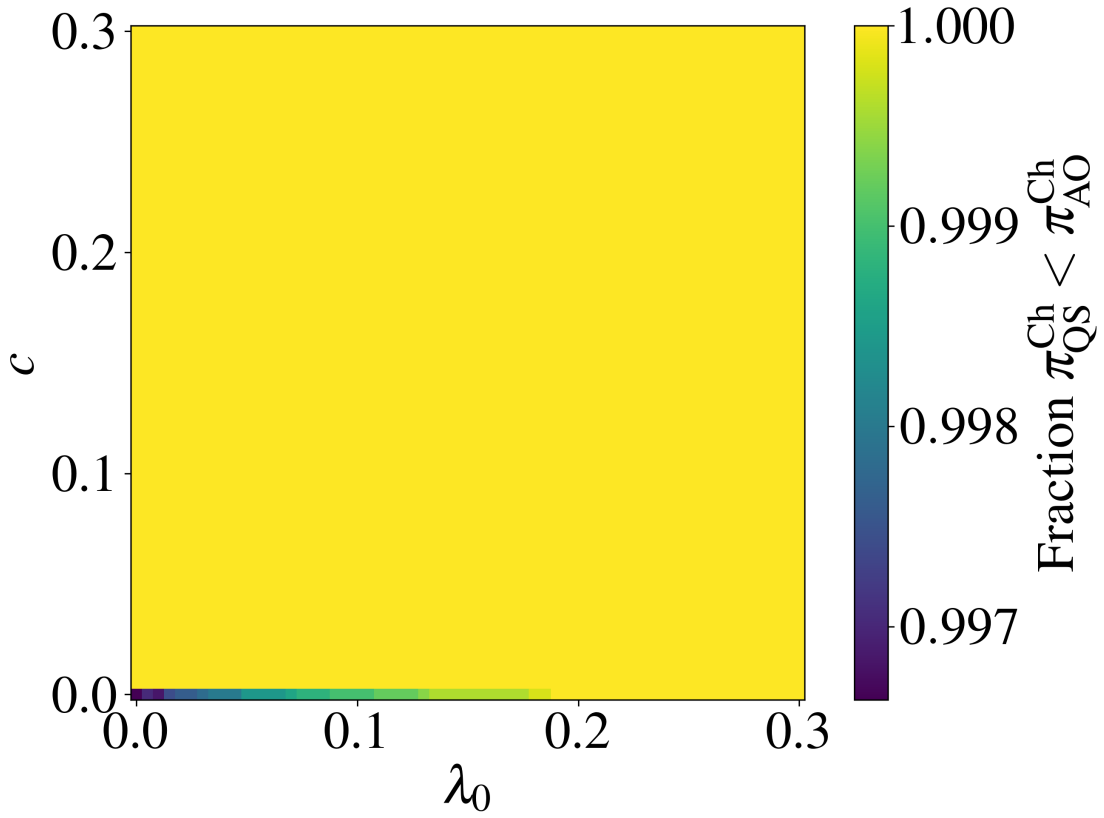

Figure S7: Phase diagram describing the fitness gains of QS over AO as a function of constitutive growth rate (λ_0) and public good production cost (c). For each pair (λ_0, c) we calculated the cheater fixation probability for all (n, m) pairs satisfying $n \geq 0$, $m \geq 0$, and $n + m \leq 100$ with the QS and AO strategies. The reported number is the fraction of these (n, m) pairs where the cheater fixation probability for QS is less than for AO ($\pi_{n,m}^{QS} < \pi_{n,m}^{AO}$). For all (λ_0, c) pairs except for when $c = 0$, cheater fixation probability is reduced by QS for all initial population compositions. When $c = 0$, there are a small number of initial compositions where $\pi_{n,m}^{QS} \geq \pi_{n,m}^{AO}$ which decreases as λ_0 increases. See Table S2 for parameter values.

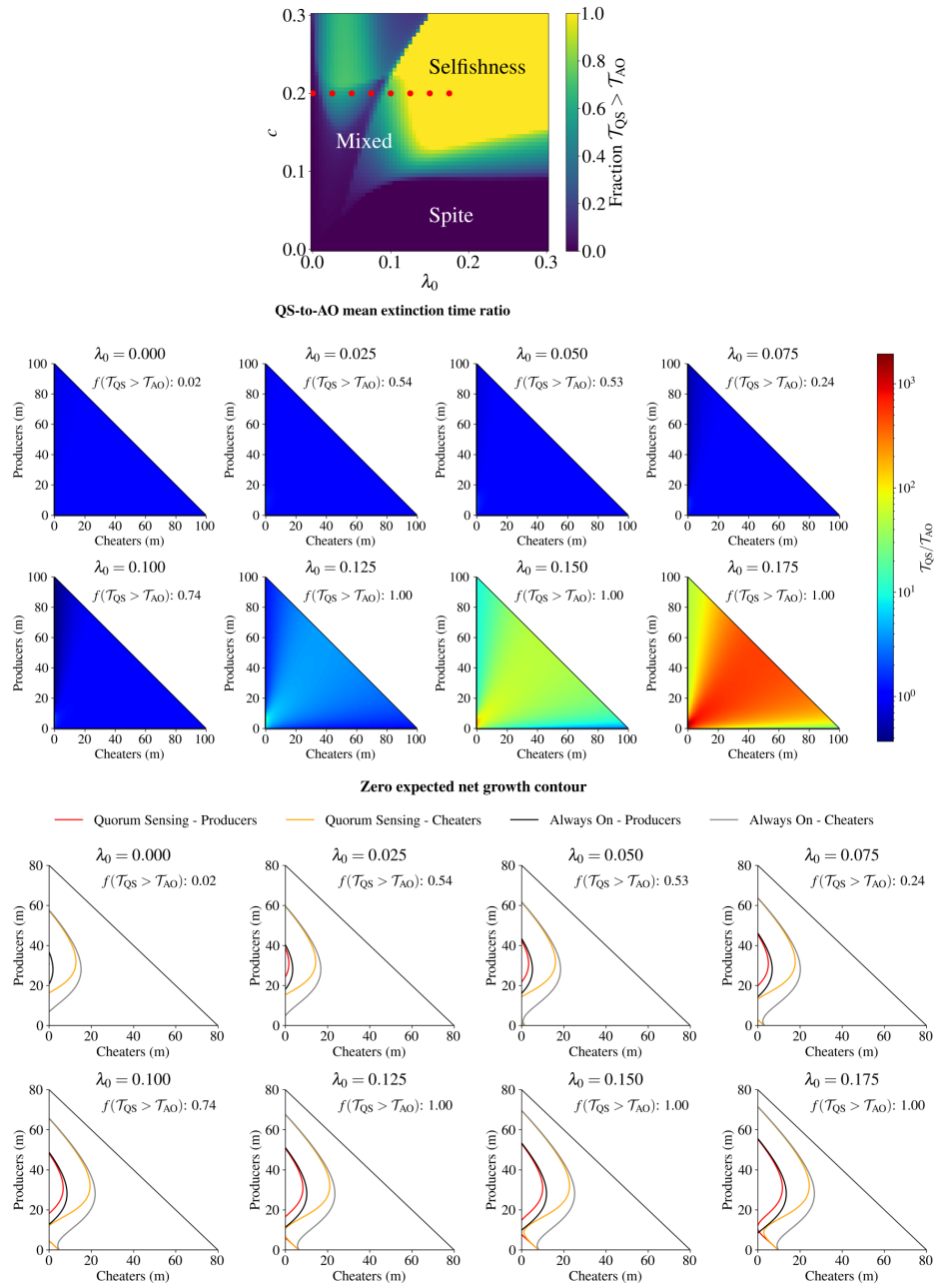

Figure S8: Detailed analysis of the phase diagram from Fig. 1 with $c = 0.2$ fixed and with different λ_0 values. Top row: the red dots shown over the phase diagram indicate the (c, λ_0) pairs that we examine in detail. Middle row: the ratio of QS mean extinction time to AO mean extinction time ($\mathcal{T}_{QS}/\mathcal{T}_{AO}$) with the indicated values of λ_0. The fraction of (n, m) pairs where ($\mathcal{T}_{QS} > \mathcal{T}_{AO}$) is indicated as $f(\mathcal{T}_{QS} > \mathcal{T}_{AO})$. Bottom row: the zero expected net growth contour contours for QS producers (red), QS cheaters (orange), AO producers (black), and AO cheaters (grey). For $\lambda_0 = 0$ the two QS zero expected net growth contour contours are identical and the two AO zero expected net growth contour contours are also identical. As λ_0 is increased, the AO producer contour approaches the producer axis faster than the QS producer contour. See Table S2 for parameter values.

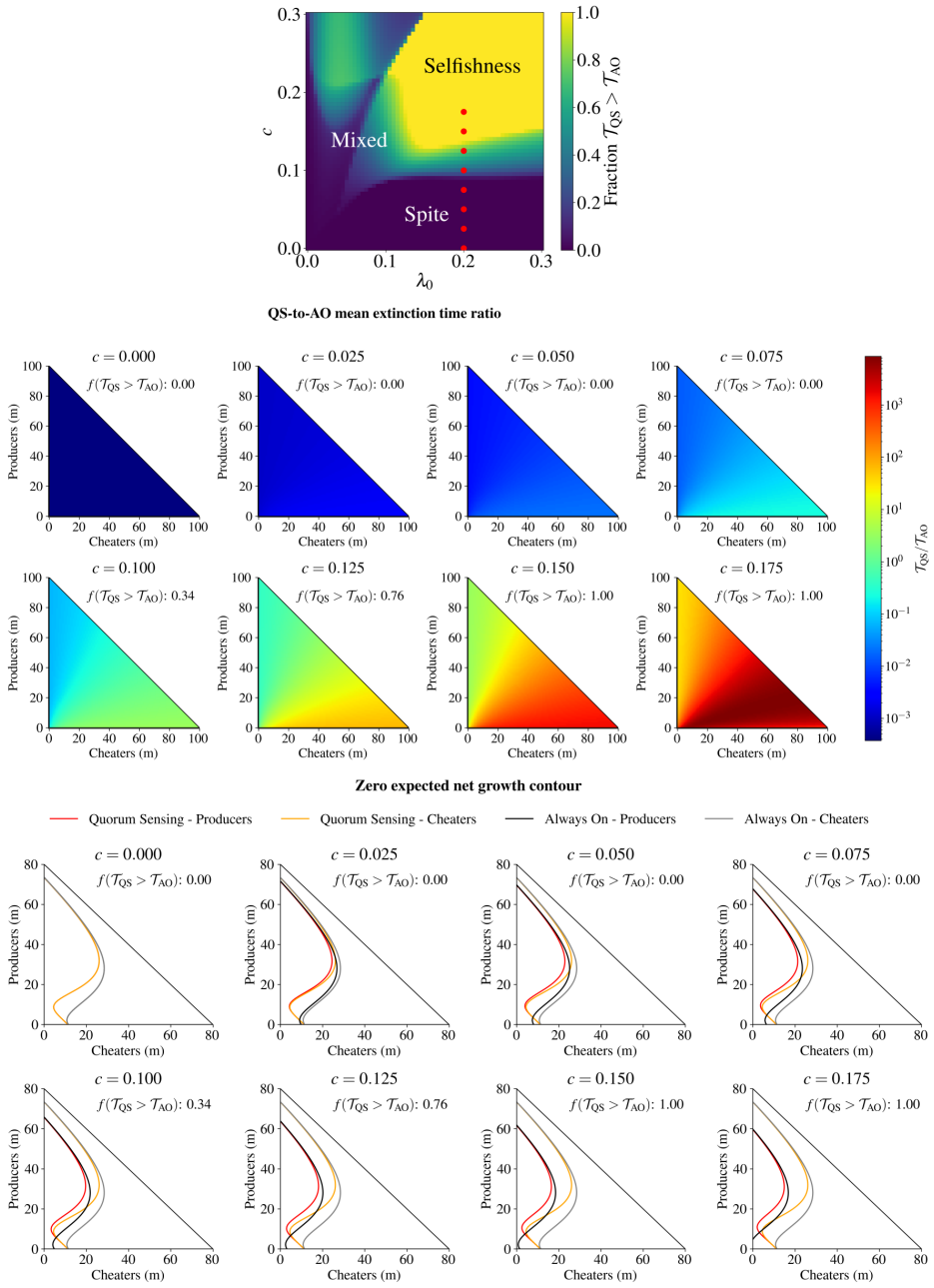

Figure S9: Detailed analysis of the phase diagram from Fig. 1 with $\lambda_0 = 0.2$ fixed and with different c values. Top row: the red dots shown over the phase diagram indicate the (c, λ_0) pairs that we examine in detail. Middle row: the ratio of QS mean extinction time to AO mean extinction time ($\mathcal{T}_{QS}/\mathcal{T}_{AO}$) with the indicated values of c. The fraction of (n, m) pairs where ($\mathcal{T}_{QS} > \mathcal{T}_{AO}$) is indicated as $f(\mathcal{T}_{QS} > \mathcal{T}_{AO})$. Bottom row: the zero expected net growth contour contours for QS producers (red), QS cheaters (orange), AO producers (black), and AO cheaters (grey). At $\lambda_0 = 0.075$ the diagonal zero expected net growth contour contour near the origin appears for QS, and moves further from the origin as λ_0 increases from there. See Table S2 for parameter values.

Table S1: Model parameters used in main text figures.

Parameter (Unit)	Figure 1	Figure 2	Figure 3	Figure 4
λ_0 (1/time)	Variable	0.0	0.2	0.2
μ_0 (1/time)	0.015	0.015	0.015	0.015
g (1/time)	1.0	1.0	1.0	1.0
c (1/time)	Variable	0.1	0.15	0.15
K_g (unitless)	20.0	20.0	20.0	20.0
h_g (unitless)	2.0	2.0	2.0	2.0
K_a (unitless)	15.0	15.0	15.0	15.0
h_a (unitless)	4.0	4.0	4.0	4.0

Table S2: Model parameters used in supplemental figures.

Parameter (Unit)	Figure S1	Figure S2	Figure S3	Figure S4	Figure S5	Figure S6
λ_0 (1/time)	0.0	0.0	0.0	0.2	0.2	0.2
μ_0 (1/time)	0.015	0.015	0.0075	0.015	0.015	0.0075
g (1/time)	1.0	1.0	1.0	1.0	1.0	1.0
c (1/time)	0.1	0.1	0.1	0.15	0.15	0.15
K_g (unitless)	20.0	20.0	40.0	20.0	20.0	40.0
h_g (unitless)	2.0	2.0	2.0	2.0	2.0	2.0
K_a (unitless)	15.0	15.0	30.0	15.0	15.0	30.0
h_a (unitless)	4.0	4.0	4.0	4.0	4.0	4.0

Parameter (Unit)	Figure S7	Figure S8	Figure S9
λ_0 (1/time)	Variable	Variable	0.2
μ_0 (1/time)	0.015	0.015	0.015
g (1/time)	1.0	1.0	1.0
c (1/time)	Variable	0.2	Variable
K_g (unitless)	20.0	20.0	20.0
h_g (unitless)	2.0	2.0	2.0
K_a (unitless)	15.0	15.0	15.0
h_a (unitless)	4.0	4.0	4.0